

An infrared laser-based reflectometer for low reflectance measurements of samples and cavity structures

Jinan Zeng and Leonard Hanssen
National Institute of Standards and Technology
100 Bureau Drive, Gaithersburg, MD, USA 20899-8441
Email: jzeng@nist.gov; Tel: 301-975-4473, Fax: 301-975-6991

ABSTRACT

An instrument, the Complete Hemispherical Infrared Laser-based Reflectometer (CHILR), has been designed and built for the accurate characterization of the total reflectance of highly absorbing samples and cavity structures down to the level of 10^{-5} . The design of CHILR employs a number of the same features of Total Integrated Scatter (TIS) measurement devices, but is used for total reflectance (both specular and diffuse components), rather than only the diffuse component. A number of features of CHILR include spatial uniformity and angular dependence of reflectance measurement capability, multiple wavelength laser sources, and the ability to measure a wide range of sample sizes and cavities with aperture sizes, ranging from 3 mm to 51 mm. We address several basic issues of alignment, background and externally scattered light, reference measurement, and laser drift, for the CHILR. We also present results of several examples, including cavities for blackbody sources, and radiometer cavities.

Keywords: Complete Hemispherical Infrared Laser-based Reflectometer, gold-coated integrating sphere, low reflectance measurement, indirect emissivity, OPO tunable laser, stabilized CO₂ laser, blackbody cavity, radiometer cavity

1. INTRODUCTION

For applications of blackbody cavity, radiometer cavity and radiometer characterization, the Complete Hemispherical Infrared Laser-based Reflectometer (CHILR)^[1, 2] was built for the accurate characterization of the total reflectance of highly absorbing samples and cavity structures at the low signal level of 10^{-5} . It is of similar design concept to the Total Integrated Scatter instrument. The CHILR possesses a number of features such as spatial uniformity and angular dependence of reflectance measurement capability. Current available multiple wavelength laser sources include diode lasers at 785 nm, 1.32 μm (1320 nm), and 1.55 μm (1550 nm) and a stabilized CO₂ laser at 10.6 μm (10600 nm)^[3]. With an OPO tunable laser^[4], its wavelength can be tuned from 1 to 5 μm . It also has the ability to measure a wide range of sample sizes and cavities with aperture sizes, ranging from 6 mm to 51 mm, as well as samples/cavities of varying weight up to 10 Kg by using a variety of translation stages. These stages provide a capability for the measurement of spatial uniformity of reflectance that provides information of the entire sample area of interest rather than a limited spot. The overall reflectance of the sample can be obtained from integration over the spatial map of the reflectance. The angular dependence measurement obtained by use of a rotation stage provides reflectance for practical scenarios and examination of fine structure in a specific direction. The basic measurement issues for CHILR are alignment, background and externally scattered light, reference measurement, and laser drift. These are examined in the following Sections, along with results of several examples, including cavities for blackbody sources, radiometer cavities for solar irradiance measurement, and a domed coated pyroelectric detector.

For accurate low-level reflectance from a blackbody cavity, both a low background and background subtraction are important. The laser-based CHILR measurement provides a comparison reference and compensation measurement for FTIR. The reflectance measurements with CHILR are applied to indirectly characterize the IR emissivity of different black body cavities. The spatial mapping of reflectance provides detail that can be correlated to structures or defects within the cavity. Empty aperture background measurements, subtracted from the apertured cavity results are used to remove the contributions of scattered and diffracted light to the measured signal and are crucial to obtain accurate reflectance values. The angular dependence of reflectance provides the information required for use of the cavities in

applications with varying imaging optics. With the additional incorporation of a tunable laser source, the reflectometer system's spectral coverage is being extended to include the 1 to 5 μm range.

2. INSTRUMENT AND EXPERIMENT DESCRIPTION

The CHILR instrument consists of a gold-coated integrating sphere of 200 mm in diameter, sample and integrating sphere manipulation stages such as translation and rotation stages, multiple wavelength lasers and OPO tunable laser source with optics of beam manipulation, detection including several detectors and a lock-in preamplifier, and reference standards.

2.1 Gold-coated integrating sphere

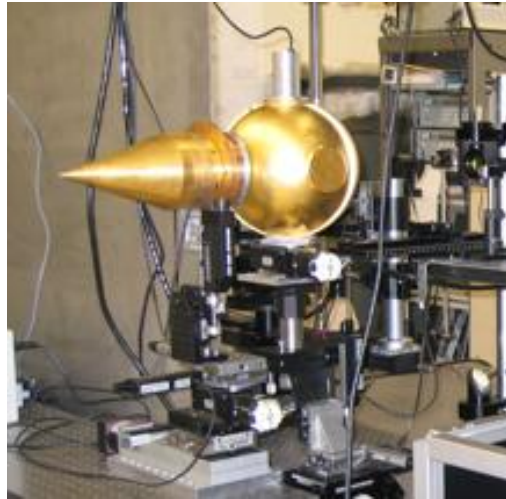


Fig. 1 Photograph of CHILR

The 203 mm dia. gold coated integrating sphere of CHILR makes use of small entrance ports. This is designed to maximize the portion of the hemisphere over which the reflected light is collected, and minimize retro-reflection loss. This is especially important for the measurement of cavity structures, where most of the reflected energy is concentrated back along the central axis of the cavity. In Fig. 1, the photograph shows the gold-coated integrating sphere and a water bath blackbody cavity. There are two entrance ports, one is a 6 mm diameter circular opening and the other is a slot opening of 6 mm wide and 24 mm long. The slot entrance opening, in combination with a rotation stage, enables spatial mapping of reflectance for cavities up to 51 mm in diameter, without loss of cavity reflected light. Even with small entrance ports, and very low reflectance samples or cavities, a sufficient signal-to-noise ratio can be obtained with the available laser power. There are three exit ports of 51 mm diameter as shown in Fig 1, two ports are in the horizontal plane and the 3rd is on the top of sphere. They are used as detector and sample ports. For the reflectance measurement, the laser beam is input into one of the entrance ports directly opposite to a 51 mm diameter sample port.

2.2 Manipulation system

The photo of the measurement setup for the large area water bath blackbody cavity in Fig. 1 shows the sample cavity mounted separately from the integrating sphere, both of which are mounted on motorized multi-axis stages. The stages consist of X-Y translation for positioning and scanning of the cavity, as well as Z translation for adjustment of the cavity aperture separation from the sphere port and rotation about the entrance aperture, allowing alignment and measurement of the angular dependence of the reflectance. The integrating sphere is also configured with X-Y translation and rotation stages for alignment, characterization and reference measurements.

2.3 Multiple wavelength lasers and OPO tunable laser

Two tunable IR laser sources are used: a periodically poled LiNbO_3 (PPLN) optical parametric oscillator (OPO), pumped by a mode-locked Nd:YVO_4 laser with a pulse duration of 7.5 ps and the repetition rate of 220MHz, and a LBO OPO pumped by the second harmonic of the Nd:YVO_4 laser. The PPLN OPO tunable laser covers wavelengths from 1350 to

5000 nm, and the LBO OPO laser tunes from 700 nm to 2000 nm with output power levels from several hundred mW to 1 W. Additional sources include, cw CO, CO₂ and isotope CO₂ lasers, with wavelength ranges of 5 to 7 μm, 9 to 12 μm, and 8 to 11 μm, respectively. All measurement results are for unpolarized light, either the average of data taken with vertical and horizontal polarized input light, or using circularly polarized input light.

An interface optics system, consisting of lenses, mirrors, polarizers, retarders, filters and a chopper are used to appropriately modify the beam power and geometry for use with the CHILR setup.

2.4 Detection system

The detection system of CHILR consists of a pyroelectric detector (top mounted), a liquid nitrogen (LN₂) cooled Mercury Cadmium Telluride (MCT) detector (side mounted) and a Germanium (Ge) detector (top mounted), with individual preamplifiers, and a lock-in amplifier. In this paper, two wavelengths of 1.32 and 10.6 μm are used for measurement. The pyroelectric detector is able to cover the entire range of interest from 1.32 μm to 10.6 μm, however, the LN₂ cooled MCT detector and the Ge detector are used to increase the sensitivity of measurement for 10.6 μm and 1.32 μm, respectively. Low reflectance measurements require a large dynamic range of detection between the reflected and input flux measurements. Use of the top-mounted pyroelectric detector for the reference measurement and the side-mounted MCT detector for the reflected flux measurement is necessary to avoid error due to nonlinearity at 10.6 μm. At 1.32 μm, the calibrated Ge detector is linear for all measurements. Through optimization of the laser beam size, a background signal can be achieved to be 4.5×10^{-5} of input with an MCT detector at 10.6 μm and about 2×10^{-3} of input at 1.32 μm with a Ge detector.

2.5 Reference standards

The sphere reflectance measurements are performed relative to diffuse and specular gold standards, calibrated at the NIST Fourier Transform Infrared Spectrophotometry Facility. This provides absolute values of reflectance (emissivity) for the samples and cavities under measurement. There are several alternative ways to perform the reference measurements. For the measurements described here, we use the substitution mode. In this case we separately characterize the sphere throughput change and correct for it.

2.6 Measurement procedure

The cavity reflectance measurement procedure is shown Fig. 2 (a)-(d).

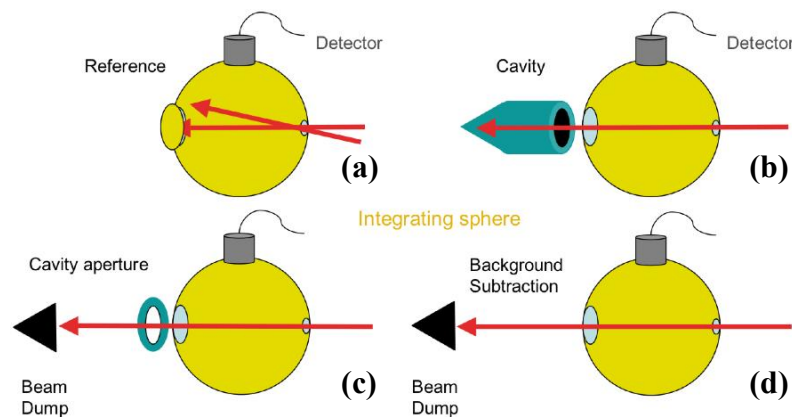


Fig. 2 Schematic of the CHILR measurement setup.

2.6.1. Reference measurement/total input flux measurement

The measurement in Fig. 2 (a) is the reference or total input flux measurement with either a previously calibrated gold standard or the port cover with the same coating as the sphere wall. Measurements are made of the reference and off the sphere wall.

2.6.2. Sample cavity measurement

The sample cavity measurement is shown in Fig. 2 (b). The reflectance measurement is performed in a directional-hemispheric geometry in the near-normal direction. This is to obtain the property of interest for cavities: the effective directional emissivity (or absorptance) in the normal direction. The sample cavity is placed as close as possible against the exit port of the integrating sphere. However, a small gap (0.5 to 1 mm) is left for the motion of sample cavity relatively to the sphere. Both the reflection signal inside and outside of the sample cavity contributes to the total reflected signal level.

2.6.3. Aperture and background measurements

As shown in Fig. 2 (d), a background measurement of the light incident in the integrating sphere or on the outside of the aperture of the cavity is made by removing the cavity and the beam incident on a distant black surface. For the low reflectance measurement, it is important to dump the beam in such a way as to insure that the return signal lower than that of the blackbody cavity. A diffuse black fiber cloth is used as a dump, with reflectance below 0.005, and is placed 2 meters behind the integrating sphere. Even if the background signal dominates the cavity signal, the cavity reflected component can still be accurately obtained by subtracting the contribution due to the aperture and scattered light collected in the sphere. For high emissivity cavities with apertures smaller than the sphere sample port (51 mm), the background measurement must be performed with an “empty” aperture in place, as shown in Fig 2 (c). It requires very precisely maintaining and/or repeating the position of the aperture between sample cavity and aperture measurements. The low reflectance level of both the sample cavity and the empty aperture and holder results in only a very small change in sphere throughput.

2.6.4. Reflectance determination

The following equation is used to determined the reflectance of sample cavity:

$$R = \frac{V_{sc} - V_{ap}}{V_r - V_{back}} R_r \quad (1)$$

Where V_{sc} is the signal from the sample cavity, V_{ap} is the signal from the aperture only, V_r is the signal from the reference material or sphere wall, V_{back} is the signal from the background, and R_r is the reflectance of the reference material.

2.7 Description of measured samples

Some examples of blackbody and radiometer cavities measured are listed in Table 1.

Table 1. List of the cavities measured

BB Cavity	Reflectance		Emissivity	
	1.32 μm	10.6 μm	1.32 μm	10.6 μm
Water Bath BB		0.00005		0.99995
Water Heat Pipe		0.00012		0.99988
Ga FP BB	0.00009	0.00005	0.99991	0.99995
Cs heat pipe		0.00062		0.99938
Small cone	0.00047	0.00167	0.99953	0.99833
Large cone	0.00009	0.00045	0.99991	0.99955
Vg cavity	0.00014	0.00646	0.99986	0.99354
HVBB	0.000045	0.00005	0.999955	0.99995
SSEC	0.00005	0.0001	0.99995	0.9999
Radiometer cavity	Reflectance			
	1.32 μm	10.6 μm		
Solar irradi. 1		0.00092		
Solar irradi. 2		0.02549		
ACR 1		0.00075		
ACR 2		0.00038		
ACR 3		0.00055		

The cavities/samples measured cover a variety of sizes from 5 mm to 1 m long and aperture diameters from 3 mm to 76 mm. Spatial uniformity measurements of the different sized cavities require either heavy duty horizontal and vertical translation stages for the large cavities or small XY stages for the small cavities. As mentioned in Sec. 2.3, often we need to perform the aperture only measurements. The maximum cavity aperture size allowed for accurate cavity measurements is 51 mm, the exit port diameter on the integration sphere. This also limits the scanning range for spatial uniformity evaluation. Qualitative information can be obtained for cavities with larger apertures, but the reflectance values must be corrected using assumptions about the spatial distribution of the cavity reflected light. The minimum cavity aperture size is dependent on the minimum size of the focused laser beam and the ratio between the cavity reflected signal and the background signal.

3. RESULTS AND DISCUSSIONS

3.1 Evaluation of the CHILR System

The CHILR system has been tested at the two wavelengths of 1.32 and 10.6 μm . The evaluation measurements include beam profiles at the front entrance and the back exit, background measurements with a beam dump, total input flux measurement, and noise floor. The performance of the CHILR system can be improved by reducing scattered light from the entrance port edge and stray light from the optics, optimizing the beam profile, and careful alignment of the system. The evaluation results of the system measurements at 1.32 and 10.6 μm up to date are summarized below.

3.1.1 Beam alignment and spot profile

The CHILR system is aligned by scanning laser beams of different wavelengths across both the entrance port and the exit port. The entrance port is 6 mm in diameter while the exit port is 51 mm in diameter. An x scan of the entrance port is measured by moving the integrating sphere along the x -axis. For an x scan of the exit port, we rotate the integrating sphere 180 deg interchanging the positions of the entrance and exit ports. Then the sphere is positioned to center the beam on both ports. In comparison, the profiles of the port edge at 1.32 μm are steeper than those at 10.6 μm indicating a corresponding smaller spot size. The input power at 1.32 μm is less than 5 mW and the input power at 10.6 μm is adjustable up to 750 mW. The background signal levels for the geometry of the small entrance port/large exit port are more than one order lower than for the inverse geometry. It means the extended wings of the beam are measured for the geometry of large entrance port/small exit port, and not for the inverse geometry. A comparison of the data in Table 2, indicates that the exit spot size at 1.32 μm is smaller than that at 10.6 μm , but that the wings of the beam at 1.32 μm are larger than those at 10.6 μm . It is also consistent with the results of the background measurements for the 51 mm opening for the two wavelengths.

3.1.2 Throughput test

The throughput test at 10.6 μm is to measure the signal change of the reflected light from a port cover of the sphere with the same coating as the sphere by using the MCT detector. The top port (dia. 25 mm) of the sphere is opened to mount various reflectance samples, including the empty port case. As shown in Fig. 3, the signal level without top sample is about 0.488 V and the noise floor is measured around 1.27×10^{-5} V. When a sample of reflectance of 97 % is in place, the signal level goes up to 0.529 V. The throughput increase for a 25 mm opening with a 97 % reflectance sample is 8 % as compared to the empty port case. For the practical situation of a 51 mm dia. port, the throughput signal should be increased proportional to the opening area. Compensation for the throughput change is taken into account when a measurement involves two samples with different reflectance values. For cavity measurements, the difference of the cavity sample reflectance of 10^{-5} and the reference sample of about 0.97 occurs results in throughput variations that require correction.

3.1.3 Background and reference measurements

Table 2 provides the results of system tests at the wavelengths of 1.32 and 10.6 μm . The spot sizes at the entrance and exit ports shown here were measured by scanning across the 6 mm diameter aperture for the geometries described in Sec. 3.1.2. With input power levels of 3 mW at 1.32 μm and that of 7 mW for 10.6 μm , the ratio between the background and reference is 0.33 % for 1.32 μm , one order higher than that of 0.029 % for 10.6 μm . By reducing the aperture to a 25 mm diameter, the ratio between the background measurement for the 25 mm aperture and the reference, for 1.32 μm increases up to 0.41 %, while the ratio for 10.6 μm changes very little to 0.031 %. In order to measure a low reflectance

level of 10^{-5} level for a good blackbody cavity at $1.32 \mu\text{m}$, about 99.4 % of the background signal has to be subtracted out of total signal. For the case of $10.6 \mu\text{m}$ the signal to be subtracted is 85.3 %. The levels of noise are $8.0 \times 10^{-6} \text{ V}$ for

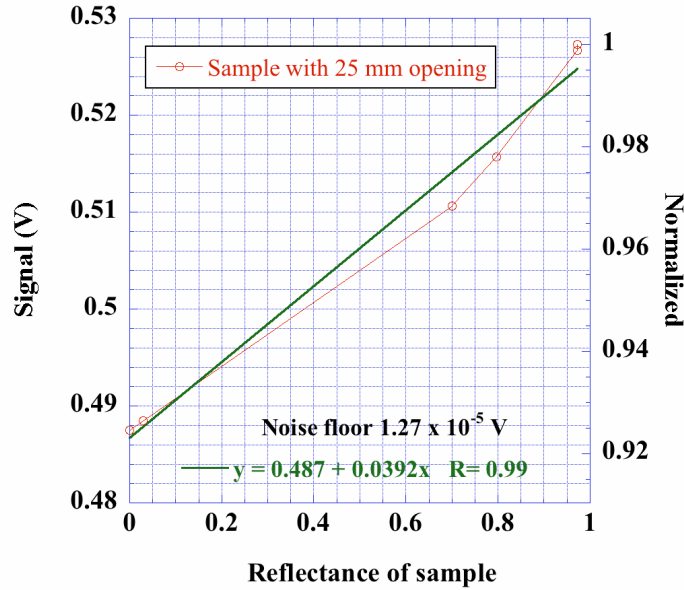


Fig. 3 The throughput test of the integrating sphere at $10.6 \mu\text{m}$

$1.32 \mu\text{m}$ and $1.87 \times 10^{-5} \text{ V}$ for $10.6 \mu\text{m}$, respectively. It means that accurate background subtraction is more significant for the measurement at $1.32 \mu\text{m}$ than that at $10.6 \mu\text{m}$.

Table 2. Summary of CHILR system measurements

	$1.32 \mu\text{m}$		$10.6 \mu\text{m}$	
Spot size (Entrance)	400 μm (FWHM) (2 mm)	Ge (gain6)	700 μm (FWHM) (2.5 mm)	Pyro
Spot size (Exit)	500 μm (FWHM) (4 mm)	Ge (gain6)	1200 μm (FWHM) (3 mm)	Pyro
Background 51 mm opening	$6.09 \times 10^{-3} \text{ V}$	Ge (gain6)	$1.44 \times 10^{-3} \text{ V}$	MCT
			$5.84 \times 10^{-6} \text{ V}$	Pyro
Aperture 25 mm Al	$7.6 \times 10^{-3} \text{ V}$	Ge (gain6)	$1.53 \times 10^{-3} \text{ V}$	MCT
			$6.23 \times 10^{-6} \text{ V}$	Pyro
Noise level	$8.0 \times 10^{-6} \text{ V}$	Ge (gain6)	$1.87 \times 10^{-5} \text{ V}$	MCT
			$2.65 \times 10^{-6} \text{ V}$	Pyro
Reference	1.8527 V	Ge (gain6)	4.9573 V	MCT
			$1.1416 \times 10^{-2} \text{ V}$	Pyro
Input power	3 mW		7 mW	
Reflectance of cavity measured	2×10^{-5}	Ge (gain6)	5×10^{-5}	MCT

3.2 Fixed point graphite cavity ($D < 51$ mm) results

3.2.1 Spatial uniformity of reflectance

A. Spatial mapping

The spatial uniformity of reflectance measurement capability is used to indirectly evaluate the emissivity of a large area cavity. The limited dimension of the entrance port and low background requirement make a large or adjustable beam impossible. A beam size of 2 mm has to be used to accomplish the low reflectance measurement for an entrance port of 6 mm in diameter. For a non-uniform sample, the averaged reflectance is needed to evaluate its emissivity rather than an individual value at a certain specific position. Sometimes the spatial variation of reflectance depends on the polarization and wavelength of light. The advantage of the spatial uniformity measurement is that in addition to the overall evaluation of reflectance, one obtains a detailed characterization of cavity surface, and is able to use the results for correction of large aperture cavities ($D > 51$ mm).

As an example of cavities with non-uniform structure, two graphite cylindrical cavities of 12 mm diameter are designed with different bottom structures: a V-groove and a cone. The angle of the cone and the V groove structure is 37° . The spatial uniformity of reflectance of the cavities was measured by scanning the sample cavities in the X-Y direction generating a spatial map. This process was repeated for the aperture only and subtracted for correction.

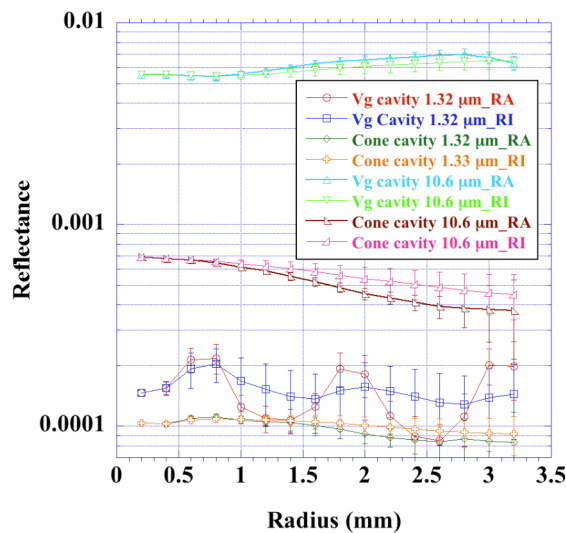


Fig. 4 Radial dependence of reflectance, averaged and integrated.

The spatial uniformity results of reflectance can be presented as a function of radius for analysis. There are two radial dependences of reflectance, averaged and integrated, shown in Fig. 4. The radially averaged result is obtained by averaging the reflectance over a ring with a constant radial increment (denoted RA). For symmetric cylinder cavity designs, this plot can give detailed radial dependence information, since the noise and local variability within the map is averaged out. The second result of the radially integrated data is calculated by averaging the reflectance over the area of the disk versus its radius. This result can be used to evaluate how a cavity's effective emissivity would depend on the viewing or irradiating geometry. The radially integrated reflectance for the maximum radius provides the reflectance of the entire aperture area of the sample cavity. Fig. 4 shows the radial averaged and integrated reflectance results at 1.32 and 10.6 μm for the graphite cylinders with V-groove and cone bottoms. The reflectance values of the V-groove cavity

within an area of 3.2 mm diameter are 0.00025 and 0.0065 for 1.32 and 10.6 μm , respectively, while those of the cone cavity over the same area are 0.00009 at 1.32 μm and 0.00045 at 10.6 μm . The radially averaged reflectance of the V-groove cavity at 1.32 μm shows the V-groove structure. The reflectance values in the valleys of the grooves are coincident with the reflectance values of the cone cavity at the equivalent locations. And the radial dependences for the two cavities show a similar trend at 1.32 μm . For 10.6 μm , the radial dependences for the two cavities present a different tendency. As the radius increases, the reflectance of the V-groove increases all the way to the 3 mm radii. However, the reflectance of the cone cavity decreases all the way to the 3 mm radius. In addition, the reflectance of the V-groove cavity at 1.32 μm shows the V-groove structure but the V-groove structure doesn't appear at 10.6 μm . The spatial maps of sample cavities provide useful information of reflectance variation for different designs rather than an individual value. The spatial uniformity of reflectance can be utilized as an input of modeling and combined with BRDF data to predict the dependence of reflectance on different geometry designs and at different wavelengths.

B. Wavelength dependence of reflectance

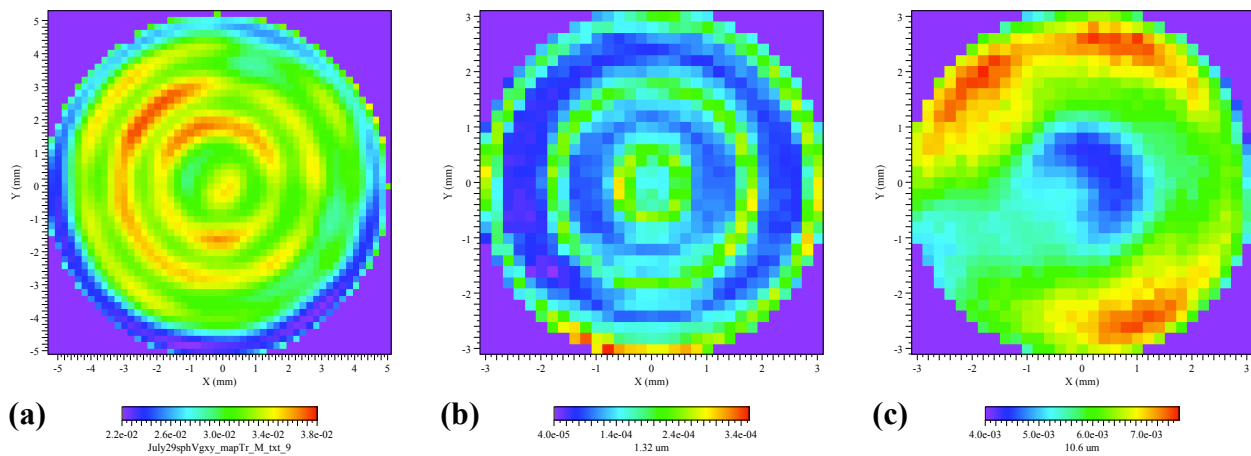


Fig. 5 Spatial maps of reflectance for the graphite groove bottom at 10.6 μm (a) the graphite cylinder with V-groove bottom at 1.32 (b) and 10.6 μm (c). Note the different spatial scale for (a) as compared to (b) and (c).

The spatial features of reflectance for the V-groove cavity at 1.32 μm are different from those at 10.6 μm . There are three graphs shown in Fig. 5. The plot (a) of Fig. 5 is the spatial map (± 5 mm) of reflectance of the graphite V-groove bottom only at 10.6 μm . The V-groove features all appear here including the central tip and rings. However, the V-maps of reflectance (on (b) of Fig. 5) at 1.32 μm shows the features of the V-groove structures (1st ring and 2nd ring) but the central tip of V-groove does not appear. The variation of reflectance at different wavelengths depends on the distribution of the reflected light in the graphite cylinder.

Bi-directional reflectance distribution function (BRDF) [5] measurements were made of representative graphite samples at 1.55 μm and 10.6 μm , shown in Fig. 6, to help understand the wavelength dependence of the spatial features of the reflectance of the V-groove cavity. The plots of Fig. 6 (a) are the BRDF results for incident angles from 0 to 71.5 deg for s and p polarized light at 1.55 μm . The curves are typical for a good diffuser. The plots of Fig. 6 (b) are the BRDF results at 10.6 μm . In contrast, there are specular peaks on the top of the diffuse components at different incident angles. The diffuse components of the BRDF at 10.6 μm are about a factor 2 greater than those at 1.55 μm . For near normal incidence, the specular component is about one order high than the diffuse component at 10.6 μm , whereas it increases to 2 orders for large angles of incidence. The V-groove or cone with 37° is equivalent to the situation of an incident angle of 71.5° for the flat surface. The dominant specular component of the BRDF for the V-groove cavity at 10.6 μm contributes to the change of the spatial features due to increased multiple reflections inside the graphite cylinder for radiation exiting the cavity aperture. For the case of 1.55 μm , the diffuse component of the BRDF for the V-groove cavity contributes to the reflected light through the aperture directly. The amount varies with the change in distance from the cavity bottom to the aperture. But the V-groove features in the spatial uniformity are maintained.

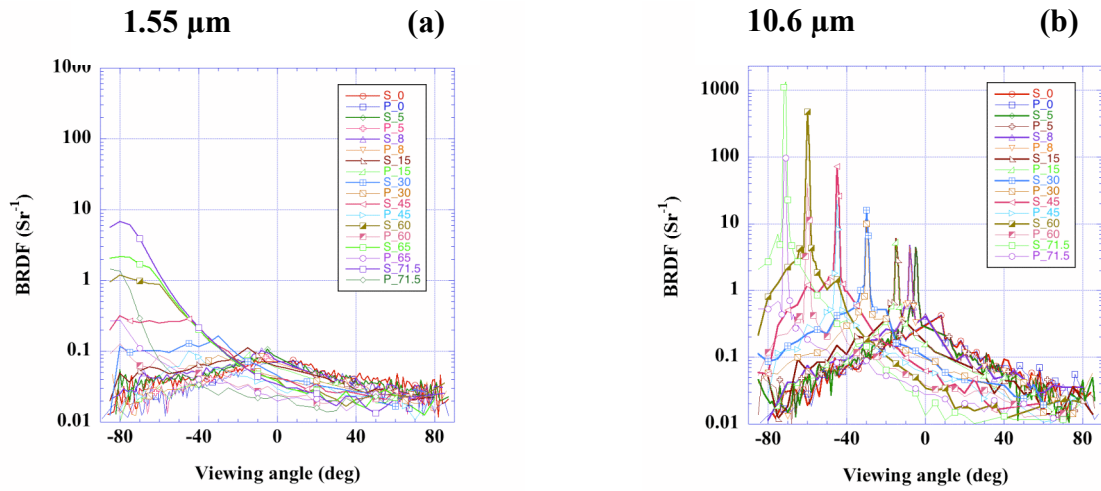


Fig. 6 BRDF of a graphite flat surface for multiple incident angles and *s* and *p* polarization, at 1.55 and 10.6 μm

C. Polarization dependence

The spatial features of the reflectance from a structured sample can vary with polarization and scanning directions. As an example, the reflected light from the graphite cylinder with V-groove bottom were measured for *s*, *p* and 45 deg. linear polarizations by scanning across the *x* and *y* directions at 10.6 μm . In Fig. 7 (a, b), the results of *x* and *y* scans at *s* and *p* polarization shows different features and the variation can be as high as 40 % due to the V-groove structure. The central peak feature of the *x* scan in *p* polarization is same as that of the *y* scan in *s* polarization since the V groove orientation and the polarization direction are same. The other configurations of the *x* scan in *s* polarization and the *y* scan in *p* polarization gives a double peak features. The average signal of *s* and *p* polarization in *x* and *y* scans are consistent with the 45 deg polarization result. To avoid polarization dependence, all other reflectance measurements are conducted in circular polarization for 10.6 μm . This demonstrates the importance of both spatial and polarized measurements.

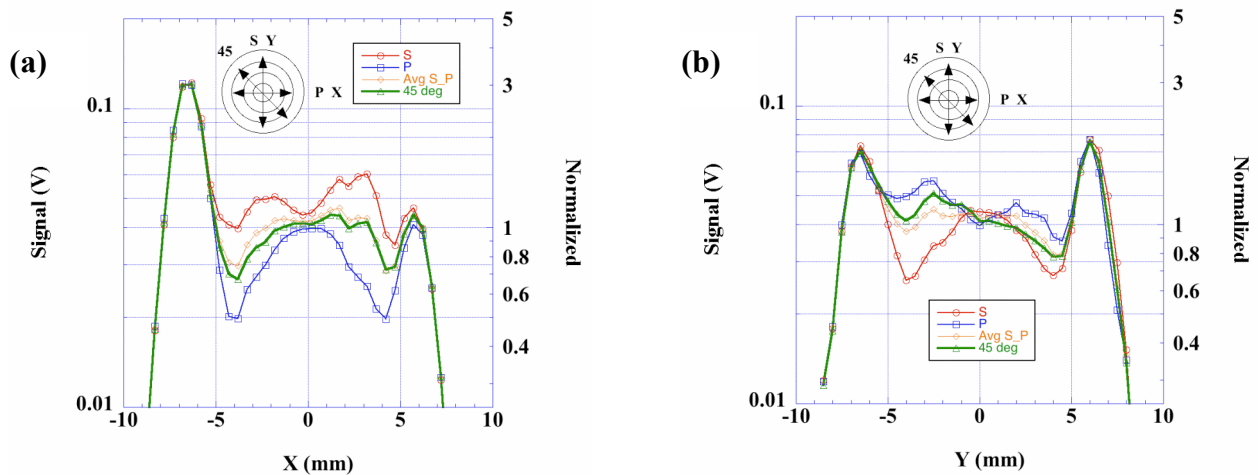


Fig. 7. Polarization dependence of the graphite cylindrical cavity with V-groove bottom at 10.6 μm .

3.2.2 Angular dependence of reflectance

The reflectance measurement of a blackbody cavity requires normal incidence of the input beam corresponding to the typical application of the cavity, which is directly viewed. The angular dependence measurement of reflectance is used to align the sample cavity, maintain repeatability of cavity positions, and to provide results for different viewing geometries. If the rotation axis is maintained at the surface of the aperture, the angular measurement can also be used to scan across the sample cavities to compare to the spatial uniformity variation.

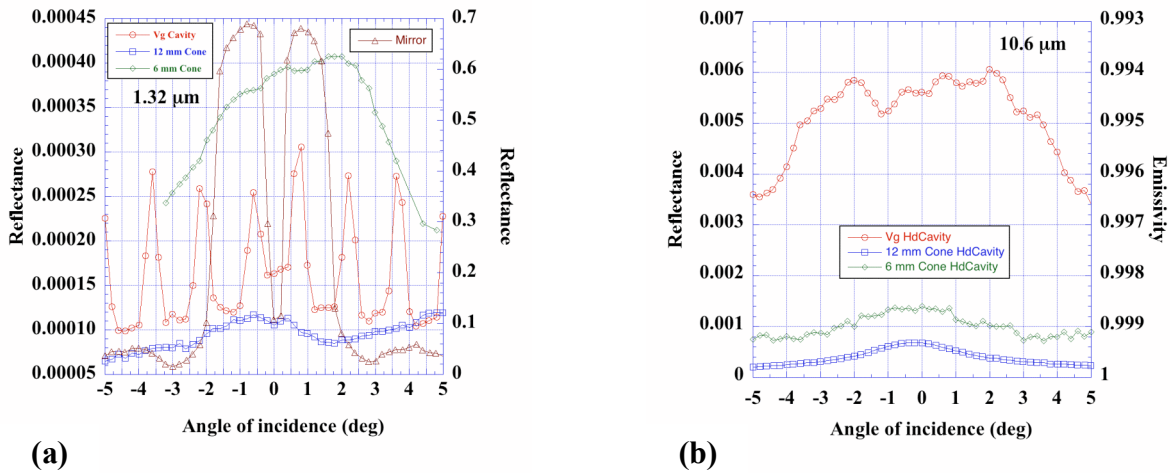


Fig. 8. Angular dependence of reflectance for the graphite cylinder with (a) V-groove and (b) cone bottoms at 1.32 and 10.6 μm.

Fig. 8 presents the angular dependence of reflectance for the graphite cavities at 1.32 and 10.6 μm. The brown triangle data in Fig. 8 (a) is a symmetric reflectance result with a mirror placed at the bottom of the graphite cylinder. The dip around 0 deg. is due to retro-reflection loss in the integrating sphere back through the 6 mm diameter sphere entrance aperture. This feature can be used to maintain the cavity alignment. When the incident angle reaches ± 1 deg, the reflectance reaches a peak of 70 % where the reflected beam from the mirror is input on the integrating sphere directly. At ± 3 deg, the reflected beam from the mirror is incident on the cavity wall. It results in a reduced reflectance at ± 3 deg. After the alignment with the mirror, the following measurements as shown on Fig. 8 (a) are for the graphite cylinder with the V-groove and cone bottoms. The angular dependence of the V-groove cavity at 1.32 μm shows the V-groove structure apparently by scanning the laser beam across the structure. The angular dependence of the cone cavity at 1.32 μm gives a peak structure. In contrast, the angular dependence of reflectance at 10.6 μm on Fig. 8 (b) presents a plateau feature for the V-groove cavity and a symmetric peak structure for the cone cavity. The small peaks of reflectance at 10.6 μm for the V-groove cavity closely match the strong peaks of the V-groove structure at 1.32 μm. The capability of angular dependence can be used for alignment and maintenance of repeatability of position, and also provides information about the spatial uniformity in situations where the reflectance cannot be measured with a linear scan.

3.3 Cs heat pipe (D = 62 mm, > 51 mm)

The cavity of a Cs heat pipe with an aperture of 76 mm in diameter provides an example of a reflectance measurement for dimensions exceeding the CHILR sphere exit port. The red curve of Fig. 9 (a) is the percentage of the overlap area to the entire area of the Cs heat pipe aperture as a function of the center offset of the two openings. The reflected light within the overlapped area can be collected by the integrating sphere. The blue curve in Fig. (a) is the missing part of the area. The overlap percentage of the area is proportional to the reflected light collected by the sphere if the distribution of reflected light is uniform. As shown, there is a 37 % loss for the geometry of entrance port (51 mm) and cavity opening (62 mm). The overlap area is constant within the range of 0 to 6 mm, above which the loss of light increases linearly as the aperture begins to miss the integrating sphere port. Another approach is to reduce the aperture of cavity. In Fig. 9 (b), the experimental and corrected results of different aperture sizes have been presented. There are three aperture sizes

(62 mm, 51 mm, 25 mm) selected for the measurement. For the 62 mm aperture, only about 63 % of the reflected light is measured assuming that the distribution of the output is uniform. The corrected reflectance takes into account both the 63 % relative area loss and the overlap loss. For the 51 mm aperture, the reflectance at the center point of zero offset is the only point measured correctly and the missing overlap area has to be corrected above 0 radius. For the case of the 25 mm aperture, there is no loss within the 51 mm opening of the integrating sphere. The radially integrated reflectance varies from 3×10^{-4} to 1.2×10^{-3} with various apertures from 25 to 62 mm.

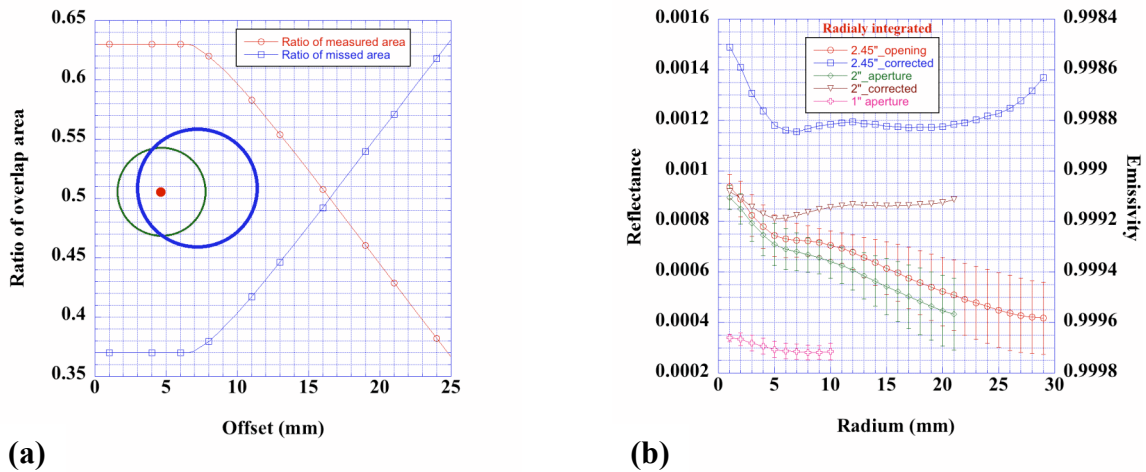


Fig. 9 Radial dependence of Cs heat pipe with a large opening and the correction calculation

3.4 Absolute Cryogenic Radiometer Cavity (D= 3 mm)

We also measured several cavities of 3 mm in diameter at the limit approaching the input beam size. Both cavity and aperture measurements were performed. Most of signal come from the surface of the aperture facing the sphere in either cavity or aperture measurement. The differences of the signals between cavity and aperture measurements are from 3 to 10 % near the center of the cavities. The cavity mounting and laser stability during the cavity and aperture measurements are crucial to accurately measure the small cavity. The reflectance is in the range of 4×10^{-4} to 7.5×10^{-4} .

3.5 Error sources and reduction methods

The major uncertainty contributions are those associated with the aperture/background measurement, reference/monitor measurement, laser stability, sensitivity and nonlinearity of the detector, sample cavity dimensions, beam profile and stray and scattered light, etc. Different cavities with wall material or coatings with various reflectance, specularly and BRDF, and measurement geometry, will produce different levels of uncertainty. The primary errors sources and related reduction approaches are discussed as follows:

1) Aperture/background measurement

The aperture/background measurements collect the reflected light from outside aperture. This part of the signal has to be subtracted from the cavity measurement. The aperture/background measurements require a repeatable position of the aperture and a high absorptance beam dump behind the integrating sphere. We use a cavity removable holder for small samples and two identical apertures with low reflectance of 0.2 % for large samples. The beam dump is a black surface located a distance of about 2 m from the sphere. Identical aperture surfaces for the empty aperture and the cavity is more crucial for the 3 mm cavity measurement. The overlap area correction method is used for large aperture cavities as shown in section 3.3.

2) Reference/monitor measurement

A reference is a standard material with known reflectance. If the reference material has a high reflectance, the throughput correction has to be taken into account as shown in section 3.1.2. There is an 8% change of throughput for an opening

area of 25 mm dia. Laser stability is vital to achieve proper comparison of measurements. Stability caused errors can be reduced by using an additional separate monitor measurement in a periodic cycle and in a substitution fashion. A certain spot on the aperture or a standard sample is used to monitor the laser drift periodically in a comparison method arrangement. A monitor method using a beamsplitter outside of the integration sphere can produce a large discrepancy of signals between the cavity and monitor measurements.

3) Sensitivity and nonlinearity of the detector

A large dynamic range is required for the measurement of low signal levels (about 10^{-5} V) from the cavity sample to the high signal level (about 1 V) from reference measurement. A combination of different detectors is used to maintain high sensitivity and avoid the nonlinear regime of certain detectors such as the MCT.

The estimated expanded uncertainty ($k=2$) for all reflectance results from the instruments, is given by

$$U = \sqrt{(0.15R)^2 + R_0^2}$$

where R is the reflectance value and R_0 is 2×10^{-5} , for the $1.32 \mu\text{m}$ results and 1×10^{-5} for the $10.6 \mu\text{m}$ results. Reflectance expanded uncertainties currently are 15 - 20% for the 10^{-3} to 10^{-5} range.

4. CONCLUSIONS

An instrument, the Complete Hemispherical Infrared Laser-based Reflectometer (CHILR), has been developed at NIST for the accurate characterization of the total reflectance of highly absorbing samples and cavity structures down to the level of 10^{-5} . A number of features of CHILR have been presented including spatial uniformity and angular dependence of reflectance measurement capability, multiple wavelength laser sources, and the ability to measure a wide range of sample sizes and cavities with aperture sizes, ranging from 3 mm to 100 mm. The system evaluation results have been discussed. We have presented the results of several examples, including cavities for blackbody sources, and radiometer cavities to show the capability of the instrument for spatial mapping, angular dependence, and wavelength dependence of reflectance measurements. Two extreme cases of a large aperture of 62 mm and small aperture of 3 mm are also presented and discussed. The measurement of the reflectance properties of blackbody cavities is a valuable tool for the evaluation of blackbody emissivity. The results have been critical to the selection and improvement of blackbodies of interest. The results obtained are complementary to those from other tools available, including Monte Carlo ray trace modelling, finite element thermal modelling analysis, and direct spectral radiance measurement comparisons with other well characterized blackbodies.

REFERENCES

- [1] Hanssen, L. M., Mekhontsev, S. N., Zeng, J., Prokhorov, A. V., "Evaluation of blackbody cavity emissivity in the infrared using total integrated scatter measurements", Proc. TEMPMEKO 2007, (2007).
- [2] Hanssen, L. M., Mekhontsev, S. N., and Khromchenko, V. B., "Infrared spectral emissivity characterization facility at NIST," *Proc. SPIE* **5405**, 1-12 (2004).
- [3] Gong, H., Hanssen, L. M. and Eppeldauer, G. P., "Spatial and angular responsivity measurements of photoconductive HgCdTe LWIR radiometers", *Metrologia*, **41**, 161-166 (2004).
- [4] Lykke, K. R., Shaw, P.-S., Hanssen, L. M., and Eppeldauer, G. P., "Development of a monochromatic, uniform source facility for calibration of radiance and irradiance detectors from $0.2 \mu\text{m}$ to $12 \mu\text{m}$ ", *Metrologia*, , **35**, 479-484, (1999) and **36**, 141-146, (1999).
- [5] Zeng, J., and Hanssen, L. M., "IR optical scattering instrument with out-of-plane and retro-reflection capabilities", Technical Digest, CLEO 05 (2005).